JOURNAL OF THE KOREAN ASTRONOMICAL SOCIETY
27: 1 ~ 11, 1994

HIGH RESOLUTION HC_3N OBSERVATIONS TOWARD THE CENTRAL REGION OF SAGITTARIUS B2

CHUNG, HYUN SOO
Division of Observational Astronomy, Korea Astronomy Observatory
AND
OHISHI, MASATOSHI AND MORIMOTO, MASAKI
Nobeyama Radio Observatory, National Astronomical Observatory, Nobeyama, Minamisaku, Nagano, Japan 384-13
(Received Dec. 15, 1993; Accepted Jan. 5, 1994)

ABSTRACT

We have observed the emission of HC_3N J=4-3, 5-4, 10-9 and 12-11 transitions toward the Sgr B2 central region in an area of 150″×150″ with resolutions of 16″-48″. The intensities and central velocities of line profiles show significant variations with positions. In contrast to the intensities of the low J-level transitions which gradually increase from the central source toward the outside region, the HC_3N emission of the high J-level transition become stronger toward the central radio continuum source MD5. Systematic change in the radial velocity of each line profile occurs along north-south direction. There are a few peaks in most line profiles, and these indicate that there are multiple velocity components along the line of sight.

Distributions of excitation temperature and column density which were estimated from the excitation calculations show the existence of a small (1×2pc), hot (T_{ex}>50K) core which contains two temperature peaks at-15″ east and north of MD5. The column density of HC_3N is (1-3)×10^{14} cm^{-2}. Column density at distant position from MD5 is larger than that in the central region. We have deduced that this 'hot-core' has a mass of $10^5M_\odot$, which is about an order of magnitude larger than those obtained by previous studies.

Key Words : interstellar molecules, HII regions, hot core, star forming regions

I. INTRODUCTION

Sgr B2 is one of the most massive molecular clouds and active star forming regions in the Galaxy. This giant molecular cloud is associated with luminous ($>10^6L_\odot$) HII regions. The central 2′ region in Sgr B2 consists of three groups of HII region that have H_2O/OH masers (Benson and Johnston 1984).

Recent molecular observations (Scoville *et al.* 1975; Churchwell and Hollis 1983; Cummins *et al.* 1983; Vanden Bout *et al.* 1983; Kuiper *et al.* 1984) toward Sgr B2 have shown the existence of warm gas in the range of 40-60K. And a hot molecular core (T_K>80K) has also been detected in the central 1′-2′ region of Sgr B2 (Solomon *et al.* 1973; Cummins *et al.* 1983).

Previous molecular line observations show that the geometrical and velocity structures of Sgr B2 are very complicated. Other studies with lower angular resolution but larger coverage show that the emission is extended over a 2′ to 6′ region and generally elongated in the north-south direction (Morris *et al.* 1976; Morris *et al.* 1977). Models of the Sgr B2 molecular cloud have been constructed by several groups (Scoville *et al.* 1975;

Morris *et al.* 1976; Avery *et al.* 1979; Vanden Bout *et al.* 1983; Lis *et al.* 1991) using different molecular line data. These models require two components to explain observed data; a small (~7pc), dense (n (H_2) ~ $10^6 cm^{-3}$) core and an extended (>15pc) low density (n (H_2) ~ $10^4 cm^{-3}$) halo. Because these observations with single dish telescope were made with poor angular resolutions (2′-3′), no detailed model for the central small (<2′) region has been made.

In this paper, we report results of high angular resolution (16″-48″) observations in four transitions of HC_3N (J=4-3, 5-4, 10-9, and 12-11) to study the spatial structure and physical parameters of the central 2′ region of Sgr B2.

In section 2 and section 3, the observational procedures and data are presented, and in section 4 model calculations and interpretation are described and the results are given in section 5.

II. OBSERVATIONS

The observations were carried out in 1993 March using 45m radio telescope of Nobeyama Radio Observatory (NRO). HC_3N J=4-3 and J=5-4 transitions were observed using a cooled single sideband (SSB) receiver with 2 GHz bandwidth, and those of J=10-9 and J=12-11 transitions were carried out using a SSB receiver with 400 MHz bandwidth, respectively. The system temperatures were 350-550K when observing Sgr B2.

The observing mode was the 'Multi On-Off' position switching method with grid spacing of 15″. The reference position of the observations is R.A. (1950.0) = $17^h44^m10^s.6$, DEC. (1950.0) = −28°22′05″. All positions reported here are expressed in ($\Delta\alpha$, $\Delta\delta$), where $\Delta\alpha$ and $\Delta\delta$ are the offsets in arcsec from the reference position in R.A. and DEC., respectively. The integration time was 5 minutes for each point. The J=4-3, 10-9, and 12-11 data were obtained at 121 positions in an area of 150″×150″. And the J=5-4 data was obtained at 71 positions in an area of 90″×150″.

Spectra were obtained with the Acousto Optical Spectrometer (AOS) with a resolution of 37kHz and a bandwidth of 40 MHz. The observed antenna temperature, T_A^*, was corrected for atmospheric attenuation by the chopper-wheel method. The rms noise fluctuations in all observations were 0.1-0.3K. In this paper, the line intensity is expressed in T_B ($T_B = T_A^*/\eta_B$ where η_B is the main beam efficiency). Table 1 lists the frequencies of the transitions observed, half-power beamwidth, main beam efficiencies, velocity resolutions, system noise temperatures, and observation dates for each lines. Pointing of the telescoped was checked by observing the SiO maser from VX Sgr and uncertainty in pointing was less than about 5″.

Table 1. Line Frequencies and Antenna Parameters

Transition	Rest Frequency (MHz)	HPBW (arcsec)	η_B (Main Beam Efficiency)	Velocity Resolution (km s^{-1})	Tsys (K)	Date
HC_3N J=4-3	36392.3654	48	0.86±0.04	0.30	550	1993 Mar. 16
HC_3N J=5-4	45490.3390	38	0.84±0.04	0.24	550	1993 Mar. 17
HC_3N J=10-9	90979.023	19	0.51±0.04	0.12	370	1993 Mar. 16
					500	1993 Mar. 18
HC_3N J=12-11	109173.634	16	0.34±0.03	0.10	550	1993 Mar. 17
					500	1993 Mar. 18

III. RESULTS

We show in Figure 1 spectra of four transitions of HC_3N. As is seen from Figure 1, line widths are generally 15km s^{-1} for J=12-11 and 20-30km s^{-1} for J=4-3. These values are generally consistent with the fact that most of the complex molecules detected in Sgr B2 cloud have linewidths of 20km s^{-1}. In fact, linewidths of HC_3N

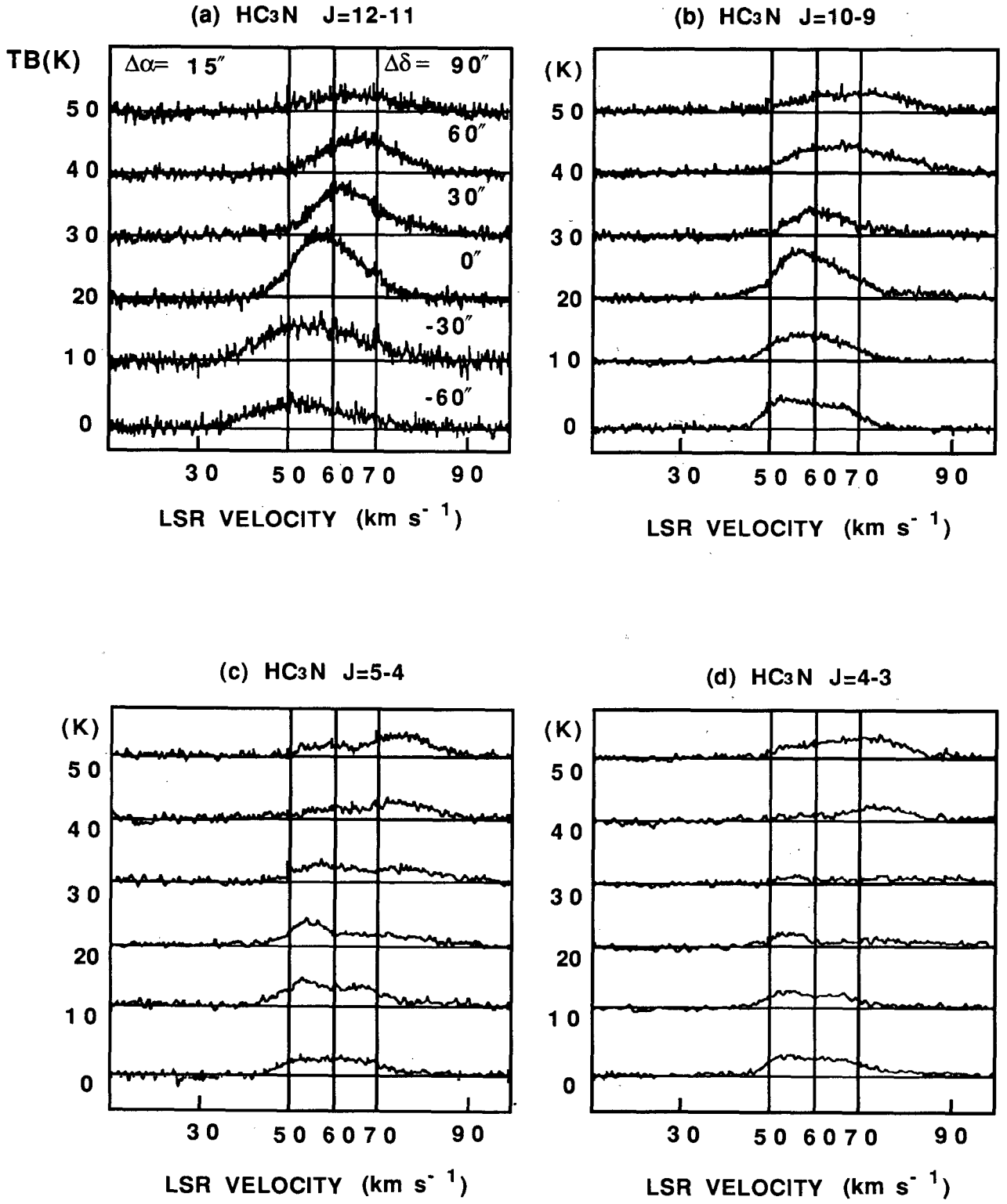

Fig. 1(a)-(d) Spectra of four transitions of HC_3N emission in the central region of Sgr B2. (a)-(d) are the spectra of HC_3N J=12-11, 10-9, 5-4 and 4-3 transitions, respectively. The position of each transition is $\Delta\delta = 15''$ and $-60'' < \Delta\delta < 90''$. The ordinate is the brightness temperature, T_B. The abscissa is the radial velocity with respect to the local standard of rest, $10 < V_{LSR} < 100$km s^{-1}. And the vertical lines in an abscissa represent that V_{LSR} is 50, 60 and 70km s^{-1}, respectively. Note the shift of peak line velocity from the position at (+15″, −60″) to the position at (+15″, +90″).

are comparable with those of the HNCO (Churchwell *et al.* 1986) and non-metastable ammonia lines (Winnewisser *et al.* 1979), ~20km s^{-1}, but are much smaller than those of CO J=1-0 lines (~65km s^{-1}, Wannier *et al.* 1976), or metastable NH_3 lines (>40km s^{-1}, Winnewisser *et al.* 1979; Morris *et al.* 1973).

From Figure 1, we show that line intensities of high-J transitions (J=12-11 and 10-9) around MD 5 is stronger than those of low-J transitions (J=5-4 and 4-3). The ratio of line intensities, (T_B (J=4-3)/T_B (J=12-11)), in this region is in general 0.2-0.3. On the other hand, when moving from center to north of south, line intensities of low J-level transitions, J=5-4 and J=4-3, increase gradually (T_B (J=4-3)/T_B (J=12-11)~0.7).

As is seen from line profiles, there exists a velocity gradient along north-south direction. For instance from Figure 1, and peak radial velocities of four HC_3N transitions change position to position: from 50km s^{-1} at (−15″, −60″) to ~65-75km s^{-1} at (−15″, 90″). This pattern of velocity gradient is consistent with those of other molecule (Morimoto *et al.* 1985; Churchwell *et al.* 1986).

Most profiles show double or multiple peak, and number of peaks vary from position to position. This suggests that more than one velocity component exists along the line of sight, and can explain some velocity variations seen in adjacent locations, but is likely to explain the velocity change over all areas observed here.

In Figure 2, we show integrated intensity maps of HC_3N J=4-3, 10-9, and 12-11. From these maps, it is apparent that the peak positions of HC_3N emission are not coincident with that of the continuum source, MD5. The emission of J=12-11 transition peaks at ~15″ west of MD5. And the emission peak of J=4-3 and J=10-9 transitions displace gradually from east to west. The position difference of emission peak between J=12-11 and J=4-3 is ~30″.

IV. DISCUSSION

1. The Excitation Calculation

In order to derive the excitation temperature and column density from the observed data of HC_3N, model calculations for the excitation of HC_3N were performed. These calculations include the lowest 20 rotational levels in the ground vibrational state of HC_3N. The hyperfine structure of these levels are determined by the Boltzmann distribution with temperature of T_{ex}.

Under this assumption, we have computed the model values of brightness temperature of HC_3N by using two parameters, T_{ex} (K), excitation temperature, and N′ ($cm^{-3}s$), column density per unit velocity interval. Model values were computed for T_{ex}=8-100K and N′=$10^{7.3}$-$10^{8.6}$$cm^{-3}s$, respectively. We obtained the model values of brightness temperature, T_B, from the following equations:

$$T_B=[T_{ex}-T_{bg}]\times[1-e^{-\tau(J+1,J)}], \tag{1}$$

$$\tau(J+1, J)=\frac{8\pi^3\mu^2N'(J+1)}{[3hUe^{\{-hBJ(J+1)/kT_{ex}\}}\times\{1-e^{\{-2hB(J+1)/kT_{ex}\}}\}]}, \tag{2}$$

where T_{bg} (=2.7K) is the temperature of the cosmic background radiation field, τ (J+1, J) is the optical depth of the transition from the J+1 to the J rotational level, m is the electric dipole moment (3.72 Debyes), U is the partition function, and others have their usual meanings. When calculating the energy levels, we ignored the influence of centrifugal distortion (D/B~10^{-7}).

Examples of comparison between model values and observed values of T_B averaged every 5km s^{-1} for each transition are plotted in Figures 3a and 3b. Open circles with error bars indicate the observed values of T_B of J=4-3, 5-4, 10-9, and 12-11 transitions in the velocity interval of 57.5<V_{LSR}<62.5km s^{-1} at a offset position (0″, 15″) and (−30″, 30″), respectively.

In Figure 3a, we show a curve (central line) that corresponds to the best-fit value of the χ^2 test and the other (upper and lower) lines show 1s deviation from the best-fit value. In some positions we could obtain only the lower limit of T_{ex} (for example (0″, 15″)) because transition with the highest brightness temperature has $J_{upper}>12$.

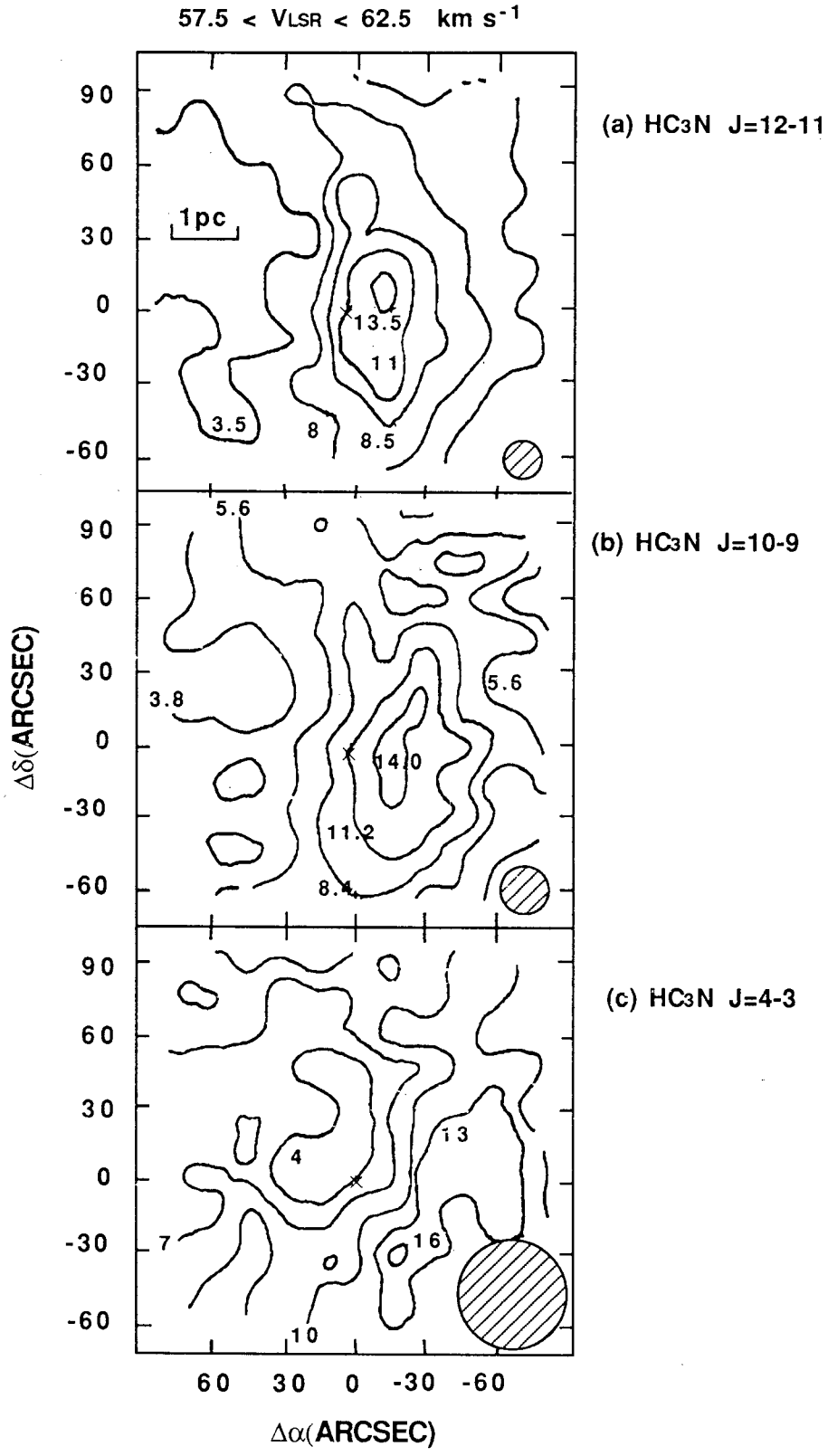

Fig. 2. Distribution of integrated line intensities of three transitions of HC_3N for $57.5 < V_{LSR} < 62.5 km\ s^{-1}$ in the central region of Sgr B2. The (0″, 0″) position corresponding to R.A. (1950.0) = $17^h44^m10^s.6$, DEC. (1950.0) = −28°22′05″, and is indicated by the cross mark. The spacing is 15 arcseconds. The lowest contour is $1K \cdot km\ s^{-1}$ and the contours are spaced by 2.5, 2.8 and $3K \cdot km\ s^{-1}$.

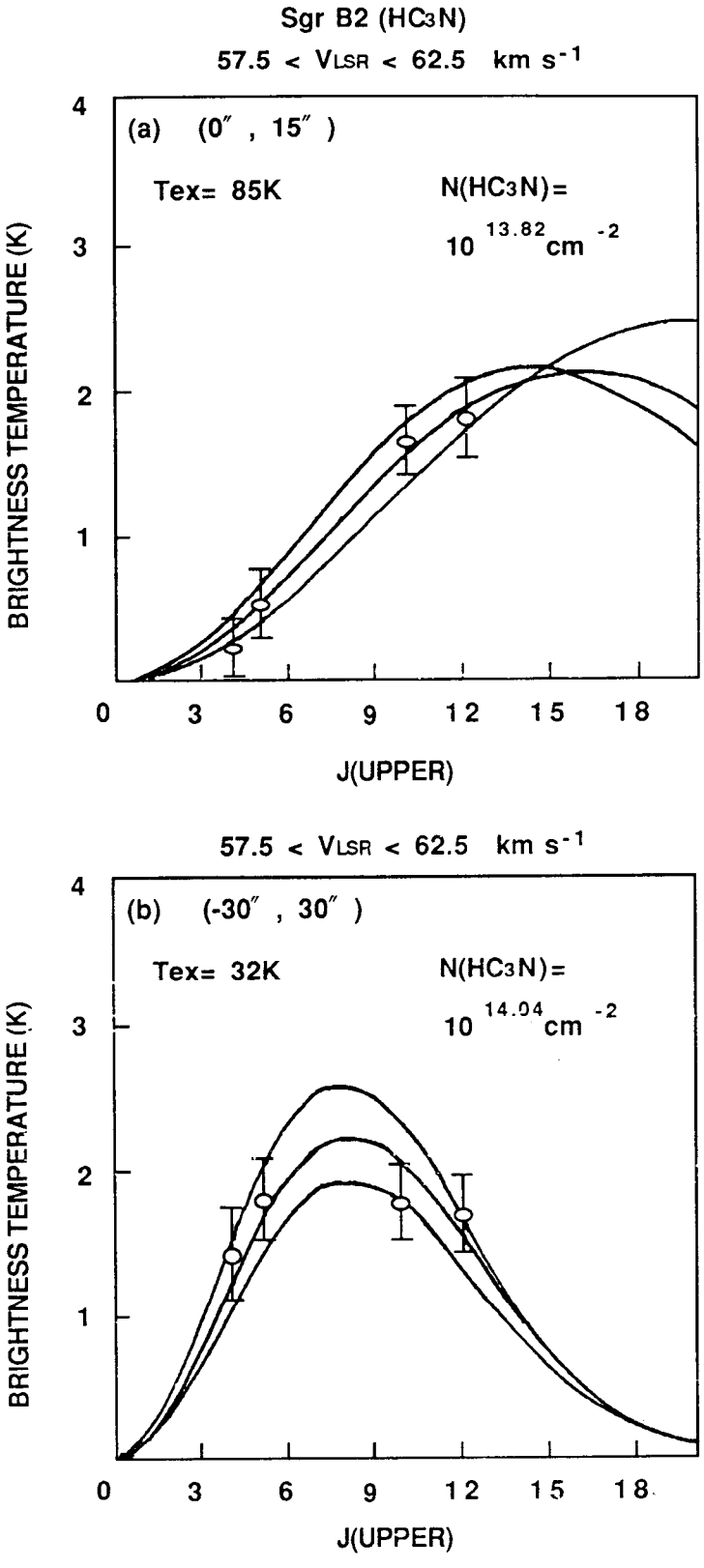

Fig. 3(a)-(b) The values of T_B versus Jupper for the Sgr B2. Open circles with error bars represent the observational data of T_B. T_B (observation) is averaged every 5km s^{-1} for each transition at the offset position of (0″, 15″) and (−30″, 30″). The best fits (solid lines) to all of the data points are compared with the upper and lower limits (dashed lines) of those.

The excitation temperature is equal to the gas kinetic temperature only when density is large enough for collisional thermal equilibrium. The transition of the higher J_{upper} level has the higher critical density, so the J=12-11 line requires the highest density among our observed four transition lines. Critical density of H_2 to excite the HC_3N J=12-11 transition is $\sim 10^6 cm^{-3}$ if we assume that the collisional rate $<\sigma v>$ is $\sim 10^{-10} cm^{-3} s^{-1}$ (Green and Chapman 1978). The average density of the central region of Sgr B2 is about $10^6 cm^{-3}$, so excitation temperature of the J=12-11 line is tend to be underestimate. Therefore, if we use the J=12-11 transition data, the derived excitation temperature tend to be lower than the gas kinetic temperature. So we can use the derived excitation temperature to know the lower limit of the gas kinetic temperature.

2. Distribution of the Excitation Temperature and Column Density

From the comparison of T_B (model) and T_B (observation) for each position, we get maps of excitation temperature (Figure 4) and column density (Figure 5). It is clear from Figure 4 that very hot ($T_{ex}>50K$) and small ($1\times 2pc$) regions are located at a position 15″ north and east of MD5 with radial velocity $\sim 60 km\ s^{-1}$ and $\sim 70 km\ s^{-1}$, respectively. And as is seen from Figures 4a, 4b, and 4c, low ($T_{ex}\sim 10$-$30K$) temperature molecular cloud are distributed in the other velocity intervals of $V_{LSR}<60 km\ s^{-1}$ and/or $V_{LSR}>70 km\ s^{-1}$ and outside regions apart from MD5.

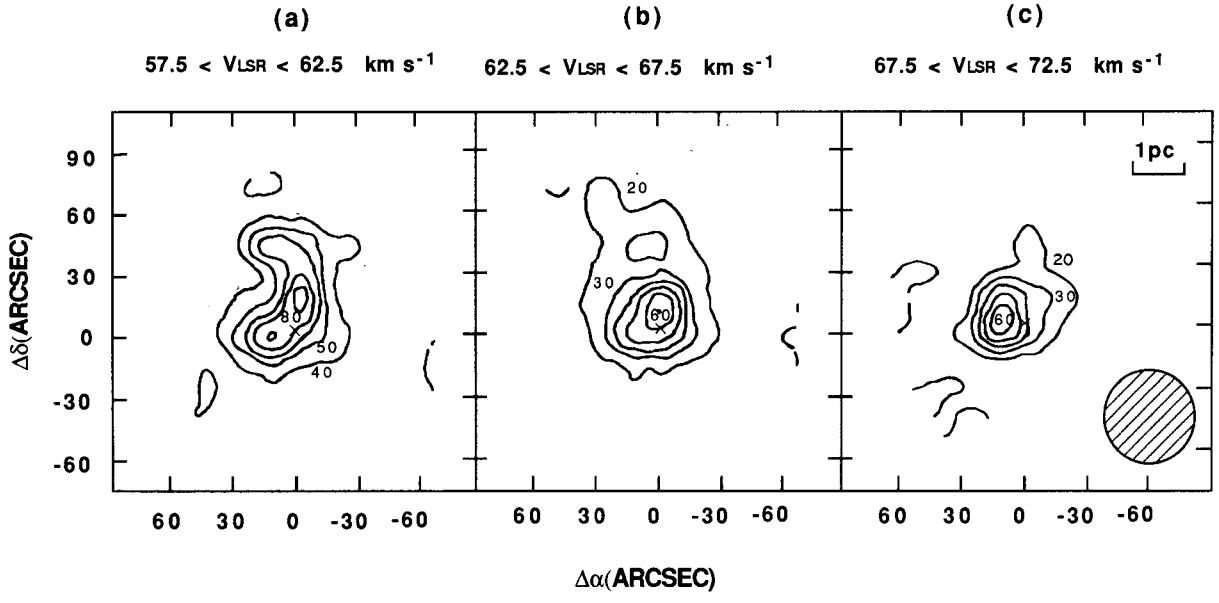

Fig. 4(a)-(c) Contour maps of excitation temperature, T_{ex}, by excitation calculations. (a)-$57.5<V_{LSR}<62.5 km\ s^{-1}$. (b)-$62.5<V_{LSR}<67.5 km\ s^{-1}$. (c)-$67.5<V_{LSR}<72.5 km\ s^{-1}$. The lowest contour is 30K, 10K, 10K, and the contours are spaced by 10K, respectively. The small and hot core structure is prominent at $57.5<V_{LSR}<62.5 km\ s^{-1}$.

The presence of a hot molecular cloud in the neighborhood of continuum peak MD5 has been indicated by observations of CH_3CN (Solomon *et al.* 1973; Linke *et al.* 1982; Cummins *et al.* 1983), and NH_3 (Winnewisser *et al.* 1979; Wilson *et al.* 1982; Vogel *et al.* 1987). In the central 1′-2′ region of Sgr B2, Solomon *et al.* (1973) and Cummins *et al.* (1983) found that $T_K\sim 100K$ and $85\pm 10K$, respectively, was required to explain the CH_3CN data. The detection of the hot gas region associated with Sgr B2 HII (M) is consistent with the expectation that molecular materials near MD5 may be heated by luminous embedded stars in it. However, the detailed structures of the hot gas region have not been resolved from the previous observations with lower spatial resolution of 1′-2′.

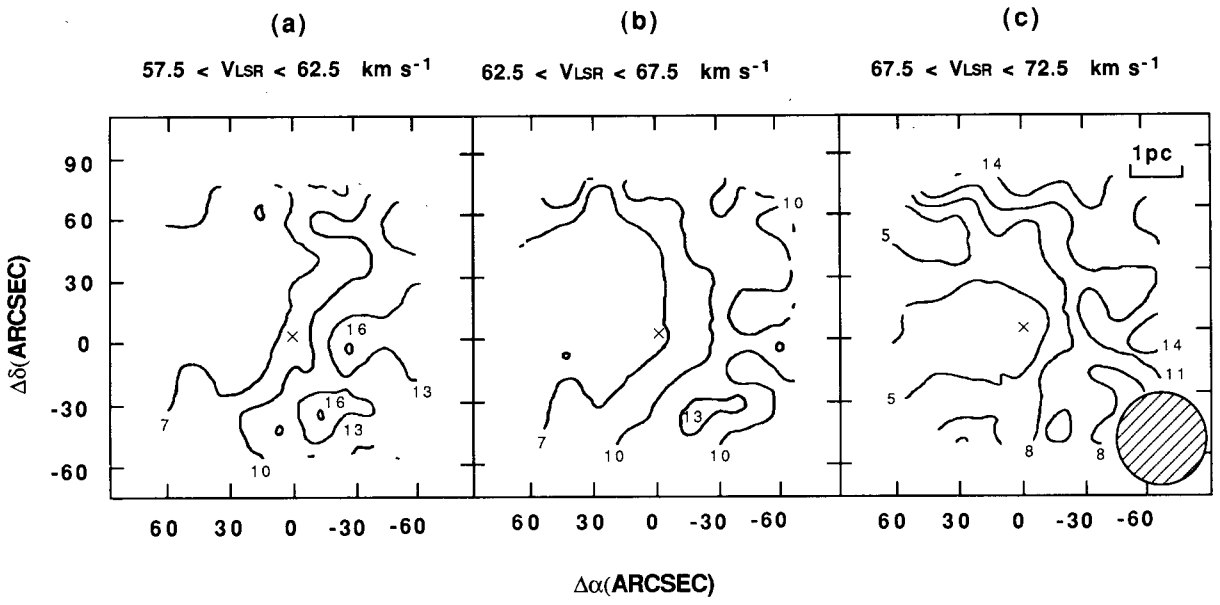

Fig. 5(a)-(c) Contour maps of column density, N (HC_3N), by excitation calculations. (a)-(c) have the same velocity intervals as Figures 4(a)-(c). The (0″, 0″) position is indicated by the cross. The lowest contour is $4\times10^{13}cm^{-2}$, $4\times10^{13}cm^{-2}$, $2\times10^{13}cm^{-2}$ and the contours are spaced by $3\times10^{13}cm^{-2}$, respectively.

We have obtained the small structure of hot molecular cloud in the central region of Sgr B2 for the first time. This hot core reported here is smaller ($\sim1\times2$pc) than those estimated by the previous studies (radius$<$5pc), and the peak of T_{ex} is not exactly consistent with MD5. We found two temperature peaks: the first peak locates $\sim15''$ north of MD5 in $V_{LSR}\sim60$km s^{-1}, and the second one locates $\sim15''$ east of MD5 and has $V_{LSR}\sim70$km s^{-1}. As will be seen later, the first peak corresponds to that of the far infrared emission. The second one has been recognized for the first time, and we could find no corresponding continuum peak and/or far infrared emission peak. When we compare the distribution of continuum emission obtained by Vogel *et al.* (1987) with that of the excitation temperature of HC_3N, we can see that two excitation temperature peaks were created through an interaction between the continuum source MD5 and surrounding molecular cloud.

In Figure 5, we show contour maps of column density for each radial velocity intervals, $57.5<V_{LSR}<72.5$km s^{-1}. As is seen from Figures 5a, 5b, and 5c, column density peaks in the south at $V_{LSR}<60$km s^{-1} and in the north at $V_{LSR}>70$km s^{-1}. These results are consistent with the fact that components of $V_{LSR}\sim50$km s^{-1} in Figure 1 are located in the south, and those of $V_{LSR}\sim70$km s^{-1} are located in the north. From the distribution of column density in Figure 5, it is shown that the column densities increase from MD5 to the outer region. This behavior would occur because ultraviolet photons from OB stars destroy molecular material near MD5 and molecules far from MD5 are shielded by dust grains from ultraviolet radiation. We obtain the column density $\sim(1\text{-}3)\times10^{14}cm^{-2}$ at almost position.

3. Mass of the Hot-Core

The extent and mass of the hot core region is estimated from the distribution of T_{ex} and N (HC_3N). From the contour map of $57.5<V_{LSR}<62.5$km s^{-1} of Figure 4, we define the 'core' region where $T_{ex}>50$K. Column density in the 'core' is approximately $(1\text{-}1.5)\times10^{14}cm^{-2}$. Therefore it seems that hot molecular materials are uniformly distributed within the 'core' region. Effective area of the core is approximately 400 $(arcsec)^2$, and its linear size is approximately $\sim1\times2$pc (assuming that the distance of Sgr B2 from the Sun is 8.5kpc).

The mass of the hot core is derived using the following method: (1) to use column densities of HC_3N, (2) to use the critical density of H_2, n (H_2), and (3) to use the virial theorem. In the first method, we use the following equation

$$M = \frac{N\,(HC_3N)_{ave} A_{eff} m\,(H_2)}{X\,(HC_3N)}, \tag{3}$$

where A_{eff} is the effective area, m (H_2) is the mass of molecular hydrogen, N $(HC_3N)_{ave}$ is the averaged column density of HC_3N within the core ($1.3\times10^{14}cm^{-2}$) and we adopted X (HC_3N) = N (HC_3N)/N (H_2) $\sim10^{-11}$ (Morris *et al.* 1976). In this calculation, we derived the mass of the core of approximately $2\times10^5M_\odot$.

In the second method, the critical density of H_2 to excite the HC_3N J = 12–11 transition in the central region of Sgr B2 is $\sim10^6cm^{-3}$, as discussed previously. The result of this calculation is $\sim3\times10^5M_\odot$. And the third method of deriving the core mass is to use the virial theorem. We find a virial mass of $\sim2\times10^5M_\odot$ by using velocity dispersion of $\sim15km\ s^{-1}$ and a core radius of $\sim1pc$.

Therefore we conclude that the small, hot core region has the mass of order of $10^5M_\odot$. This value is an order of magnitude larger than $2\times10^4M_\odot$ derived by Goldsmith *et al.* (1988) in Sgr B2 core region. Such enormous mass of the 'core' in linear scale of $\sim2pc$ is comparable to that in a typical giant cloud with size of 100pc. It is thus surprising that this enormous mass is concentrated in an extremely small 'core'. In addition, the large mass and small size of the Sgr B2 'core' region are comparable to these of W49, $(0.5\text{-}2.5)\times10^5M_\odot$ and 3.4pc, deduced by Miyawaki *et al.* (1986).

4. Comparison with Infrared Data of Hot-Core region

Since a number of far-infrared observation toward Sgr B2 have been reported, we can make a comparison between out results and those of far infrared observations. The central region of Sgr B2 appears as a strong far infrared source between 40 and 200μm. The luminosity of the core region obtained by Erickson *et al.* (1977) ($\sim10^{6.8}L_\odot$ for $40<\lambda<200\mu m$) is sufficient to maintain their immediate surrounding at a high temperature. From the observations of Benson and Johnston (1984), the Sgr B2 (M) region is powered by embedded premain -sequence stars having a total luminosity of $>10^6L_\odot$. It is interesting that the high temperature region in north peak obtained by us is coincident with the infrared source at 30μm (Nagata *et al.* 1986, private communication), 50μm (Gatley *et al.* 1978), 60μm (Thronson and Harper 1986) and 200μm (Erickson *et al.* 1977) that appears sharply peaked close to the position of the continuum source MD5.

Scoville and Kwan (1976) obtained the fact that the upper bound on the dust temperature distribution was a function of luminosity and distance. Therefore, the upper limit on the dust temperature is calculated by using equation (9) obtained by Scoville and Kwan (1976), if the following facts are assumed: first, that the dust emissivity at 50μm is 0.0019 (Hildebrand 1983), and, second, that the far infrared wavelength dependence is λ^{-1}.

The result is given by $T_d(r) = 120r^{-0.4}$ for the continuum source MD5 of luminosity $10^{6.58}L_\odot$ obtained by Benson and Johnston (1984) where T_d is the dust temperature (K) and r is the distance from the center position (pc). At the distance of 1pc and 2pc from the central source, we obtain $T_d = 120K$ and 90K, respectively, from this equation. Therefore, from the comparison of these results and the excitation temperature derived by us, an estimate of the expected source size should be less than 40″ in diameter. This size is similar to ours but is somewhat less than that of the size of 30″×60″. The most likely explanation about the small size calculated here is that the multiple heating sources may be permit high dust temperature distribution on a scale greater than that for a single heating source, probably because the multiple heating sources are spread over a more extended region (Goldsmith *et al.* 1988). At 350μm the core of the infrared cloud also overlaps the compact radio continuum sources, but seems to be slightly displaced to the north of the molecular cloud (Rieke *et al.* 1973; Righini *et al.* 1975). Similarly, strong 1mm emission has been found to peak near the compact HII regions (Westbrook *et al.* 1976). To within 1′, the 1μm emission and the 350μm emission maxima agree with the peak of the molecular emission.

Thus, within the uncertainties of position, the position of the HC_3N hot-core seems to be in good coincidence with the peak of all the far infrared observations of 40μm-350μm (Rieke *et al.* 1973; Righini *et al.* 1976; Thronson and Harper 1986), indicating that the warm dust responsible for the far infrared emission lies outside the HII region in the associated molecular cloud.

V. CONCLUSION

We have carried out high angular resolution observations of HC_3N in the central region of Sgr B2. There exists a systematic variation of peak radial velocity along north-south direction. Most profiles have two or more peaks and asymmetric shapes. This suggests that several velocity components exist along the line of sight.

We derive distributions of column density and excitation temperature of HC_3N in the radial velocity intervals $57.5 < V_{LSR} < 72.5$km s^{-1} from the model calculations. A contour map of the excitation temperature has revealed that there are two peaks in the central region and the peak position of T_{ex} are not coincident with the location of radio continuum source MD5, and are located $\sim 15''$ west and north of MD5, respectively. This behavior is also shown in the far infrared observations, and our observational results about the Sgr B2 hot-core region agree with the infrared source at 30μm-350μm within the positional uncertainties.

We have obtained that this small hot-core ($T_{ex} > 50$K) region of Sgr B2 has a smaller size of 1×2pc than those estimated by the previous studies. The estimated mass within this area is an order of $10^5 M_\odot$. It is very surprising that such enormous mass is concentrated in this small scale.

We thank all the staff of Nobeyama Radio Observatory for encouraging us during this work. This paper is supported in part by the Basic Science Research Institute Program, Ministry of Education, 1993, Project NO. BSRI93-228.

REFERENCES

Avery, L. W., Oka, T., Broten, N. M. & MacLeod, J. M. 1979, ApJ, 232, 48
Benson, J. M. & Johnston, K. J. 1984, ApJ, 277, 181
Churchwell, E. & Hollis, J. M. 1983, ApJ, 272, 591
Churchwell, E., Wood, D., Myers, P. C. & Myers, R. V. 1986, ApJ, 305, 405
Cummins, S. E., Green, S., Thaddeus, P. & Linke, R. A. 1983, ApJ, 266, 331
Erickson, E. F., Caroff, L. J., Simpson, J. P., Strecker, D. W. & Gorvitch, D. 1977, ApJ, 216, 404
Gatley, I., Becklin, E. E., Werner, M. W. & Harper, D. A. 1978, ApJ, 220, 822
Goldsmith, P. F., Snell, R. L., Hasegawa, T. & Ukita, N. 1987, ApJ, 314, 525
Green, S. & Chapman, S. 1978, ApJS, 37, 169
Hildebrand, R. H. 1983, QJRAS, 24, 267
Kuiper, T.B.H., Rodriquez Kuiper, E. N., Dickinson, D. F., Turner, B. E. & Zuckerman, B. 1984, ApJ, 276, 211
Linke, R. A., Cummins, S. E., Green, S. & Thaddeus, P. 1982, in Regions of Recent Star Formation, ed. R. S. Roger & P. E. Dewdney. (Boston: Reidel), p. 391
Lis, D. C., Carlstrom, J. E., Keene, J. 1991, ApJ, 380, 429
Miyawaki, R., Hayashi, M. & Hasegawa, T. 1986, ApJ, 305, 353
Morimoto, M., Ohishi, M. & Kanzawa, T. 1985, ApJ, 288, L11
Morris, M., Zuckermann, B., Palmer, P. & Tuerner, B. E. 1973, ApJ, 186, 501
Morris, M., Turner, B. E., Palmer, P. & Zuckermann, B. 1976, ApJ, 205, 82
Morris, M., Snell, R. L. & Vanden Bout, P. 1977, ApJ, 216, 738
Rieke, G. H., Harper, D. A., Low, F. J. & Armstrong, K. R. 1973, ApJ, 183, L67
Righini, G., Simon, M., Joyce, R. R. & Gezari, D. Y. 1975, ApJ, 195, L77
Scoville, N. Z., Solomon, P. M. & Penzias, A. A. 1975, ApJ, 201, 352
Scoville, N. Z., Kwan, J. 1976, ApJ, 206, 718
Solomon, P. M., Penzias, A. A., Jeffert, K. B. & Wilson, R. W. 1973, ApJ, 185, L63
Thronson, JR. H. A. & Harper, D. A., 1986, ApJ, 300, 396 Vanden Bout, P. A., Loren, R. B., Snell, R. L. & Wootten, A. 1983, ApJ, 271, 161
Vogel, S. N., Genzel, R. & Palmer, P. 1987, ApJ, 316, 243
Wannier, P. G., Penzias, A. A., Linke, R. A. & Wilson, R. W. 1976, ApJ, 204, 26

Westbrook, W. E., Werner, M. W., Elias, J. H., Gezari, D. Y., Hauser, M. G., Lo, K. Y. & Neugebauer, G. 1976, ApJ, 209, 94
Wilson, T. L., Ruf, K., Walmsley, C. M., Martin, R. N., Pauls, T. A. & Batrla, W. 1982, A&A, 115, 185
Winnewisser, G., Churchwell, E. & Walmsley, C. M. 1979, A&A, 72, 215